HHS Public Access

Author manuscript

IEEE Trans Biomed Eng. Author manuscript; available in PMC 2023 September 01.

Published in final edited form as:

IEEE Trans Biomed Eng. 2022 September ; 69(9): 2723–2732. doi:10.1109/TBME.2022.3150781.

An affordable and easy-to-use focused ultrasound device for noninvasive and high precision drug delivery to the mouse brain

Zhongtao Hu [Member, IEEE],

Si Chen,

Yaoheng Yang [Graduate Student Member, IEEE],

Yan Gong [Graduate Student Member, IEEE],

Hong Chen [Member, IEEE]

Department of Biomedical Engineering, Washington University in St. Louis, St. Louis, MO 63105 USA.

Department of Biomedical Engineering, Washington University in St. Louis, St. Louis, MO 63105 USA and with the Department of Radiation Oncology, Washington University School of Medicine, St. Louis, MO 63110 USA.

Abstract

Objective: Focused ultrasound (FUS) combined with microbubble-mediated blood-brain barrier (BBB) opening (FUS-BBBO) is not only a promising technique for clinical applications but also a powerful tool for preclinical research. However, existing FUS devices for preclinical research are expensive, bulky, and lack the precision needed for small animal research, which limits the broad adoption of this promising technique by the research community. Our objective was to design and fabricate an affordable, easy-to-use, high-precision FUS device for small animal research.

Methods: We designed and fabricated in-house mini-FUS transducers (~$80 each in material cost) with three frequencies (1.5, 3.0, and 6.0 MHz) and integrated them with a stereotactic frame for precise mouse brain targeting using established stereotactic procedures. The BBB opening volume by FUS at different acoustic pressures (0.20–0.57 MPa) was quantified using T1-weighted contrast-enhanced magnetic resonance imaging of gadolinium leakage and fluorescence imaging of Evans blue extravasation.

Results: The targeting accuracy of the device as measured by the offset between the desired target location and the centroid of BBBO was 0.63 ± 0.19 mm. The spatial precision of the device in targeting individual brain structures was improved by the use of higher frequency FUS transducers. The BBB opening volume had high linear correlations with the cavitation index (defined by the ratio between acoustic pressure and frequency) and mechanical index (defined by the ratio between acoustic pressure and the square root of frequency). The correlation coefficient of the cavitation index was higher than that of the mechanical index.

Corresponding author: Hong Chen, hongchen@wustl.edu.
Zhongtao Hu, Si Chen and Yaoheng Yang contributed equally to this work.

Conclusion: This study demonstrated that spatially accurate and precise BBB opening was achievable using an affordable and easy-to-use FUS device. The BBB opening volume was tunable by modulating the cavitation index. This device is expected to decrease the barriers to the adoption of the FUS-BBBO technique by the broad research community.

Index Terms—

Focused ultrasound; Blood-brain barrier; Brain drug delivery; Cavitation index; Mechanical index

I. Introduction

Focused ultrasound combined with microbubble-mediated blood-brain barrier opening (FUS-BBBO) has been established as a promising technique for the noninvasive and localized delivery of various therapeutic agents to the brain [1]. Its feasibility and safety have been demonstrated in patients with various brain diseases, including brain tumors [2]–[5], Parkinson's disease[6], amyotrophic lateral sclerosis [7], and Alzheimer's disease [8]–[11]. However, FUS-BBBO is not only a promising technique for clinical applications but also a powerful preclinical research tool that has the potential to be adopted by a broad research community, including but not limited to neuroscience, neuro-oncology, and neurology. For example, FUS-BBBO can facilitate the delivery of gene vectors encoding channelrhodopsin to the mouse brains for optogenetic neuromodulation [12] and engineered G-protein-coupled receptors for chemogenetic neuromodulation [13]. It can also modulate brain function by delivering neurotransmitters (*e.g.*, GABA [14]) to a targeted brain location. Besides these applications in neuroscience, FUS-BBBO has been used in neuro-oncology research to evaluate the delivery efficiency and therapeutic efficacy of various agents in murine models of brain tumors, such as chemotherapeutic agents (*e.g.*, BCNU [15]), monoclonal antibodies (*e.g.*, Herceptin [16] and bevacizumab [17]), and nanoparticles (*e.g.*, brain-penetrating nanoparticles [18] and radiolabeled copper nanoclusters [19]). FUS-BBBO without any drugs was found to reduce the amyloid plaque and improve cognitive performance in Alzheimer's disease mouse models [20]. FUS-BBBO can also be used to deliver therapeutic agents (*e.g.*, GSK-3 inhibitor [21]) to further reduce plaque deposition in mouse models. Despite the great promise, the adoption of FUS-BBBO by the broad research community is limited by the lack of affordable, easy-to-use, and high precision FUS devices for mouse studies.

Existing FUS devices for FUS-BBBO in mice are expensive, bulky, and have a high technical barrier. There are only a few commercially available FUS devices for preclinical FUS-BBBO research, for example, magnetic resonance imaging (MRI)-guided FUS devices provided by Image Guided Therapy (IGT, Pessac, France) [13][22], MRI- and stereotactic-guided FUS devices from the FUS Instruments Inc. (Toronto, Ontario, Canada) [23][24], ultrasound imaging-guided FUS system, such as VIFU 2000 from Alpinion US Inc. (Bothell, WA, USA) [25] and HIFUPlex from Verasonics Inc. (Kirkland, WA, USA) [26]. These commercial devices are expensive (~$50,000 to ~$250,000). There are also custom-made FUS devices, including single-element FUS transducers [27][28] and phased-array transducers [30][31]. Single-element FUS transducers have been the most widely used devices because they are more affordable than phased arrays. However, even single-element

FUS transducers are often bulky with large apertures (~50 mm). These bulky transducers require heavy 3D motors to control their positioning for brain targeting. Moreover, MRI or ultrasound imaging is often needed to guide the spatial targeting of the FUS transducer at a specific brain location, limiting the usages of FUS-BBBO to mainly groups with expertise in ultrasound and/or MRI. A stereotactic-guided FUS system was introduced by Bing *et al.* [24] and later commercialized by the FUS Instruments Inc. This system uses a stereotactic frame to stabilize the mouse head and use the brain atlas to guide the positioning of the FUS transducer, which avoids the need for MRI or ultrasound imaging guidance. However, same as all other FUS devices, the FUS transducer is bulky and the cost of the device is still high.

The broad application of FUS-BBBO in small animal research is also limited by the low spatial precision of existing FUS devices. The commonly used FUS transducers have low frequencies ($\leqslant$ 1.5 MHz) with a focal region size at the scale of $1\times1\times10$ mm^3, which essentially covers the entire depth of the mouse brain (~6 mm) [31]–[37]. Low-frequency transducers are needed to minimize skull-induced attenuation and beam aberration, which is critical in clinical applications. However, the mouse skull is much thinner than the human skull. Successful BBBO was reported using a diagnostic ultrasound imaging probe with a center frequency of 8 MHz in combination with microbubbles [38]. However, the focal region size of the ultrasound imaging probe was large, which was not suitable for spatially precise BBBO in mice. FUS transducers with optimized design are needed to precisely target individual structures in the mouse brain.

Precise control of BBBO volume and drug delivery efficiency is also needed to ensure robust application of FUS-BBBO. Both the mechanical index (defined by the ratio between acoustic pressure and the square root of frequency, MI = $P/\sqrt{f}$) and cavitation index (defined by the ratio between acoustic pressure and frequency, CI = P/f) have been proposed to evaluate the likelihood of FUS-BBBO as well as the drug delivery efficiency. McDannold *et al.* found that MI was correlated with the threshold of FUS-induced BBB opening [39]. Chu *et al.* found both MI and CI were highly correlated with the delivery efficiency of FUS-BBBO, and the correlation with MI was slightly higher than that of CI [40].

The objective of this study was to design and fabricate an affordable and easy-to-use FUS device for spatially accurate and precise FUS-BBBO. We manufactured in-house mini-FUS transducers (~$80 each in material cost) with different frequencies (1.5, 3.0, and 6.0 MHz) and integrated them with a commercially available stereotactic frame using 3D-printed parts. We found that this device achieved FUS-BBBO with sub-millimeter accuracy as measured by the offset between the desired target location and the BBBO centroid. We also showed that FUS-BBBO volume could be decreased for spatially precise BBBO by increasing the frequency or decreasing the acoustic pressure. The drug delivery volume had high linear correlations with CI and MI, and the correlation coefficient with CI was higher than that of MI.

II. MATERIALS AND METHODS

A. Design and fabrication of the FUS device

The stereotactic-guided FUS device (Fig. 1(a)) consisted of a commercially available stereotaxic apparatus; in-house manufactured miniature FUS transducers; 3D-printed transducer housing and adapter; and transducer driving system, including a commercially available function generator (Model 33500B, Keysight Technologies Inc., Englewood, CO, USA) and a power amplifier (1020L, Electronics & Innovation, Rochester, NY, USA). The stereotaxic apparatus (Model 940, David Kopf Instruments, Tujunga, California) have been widely used in neuroscience for small animal research. It has a 10-micron movement resolution for all axes and includes an easy-to-read compact digital display console.

The key hardware component was the FUS transducer. The miniature FUS transducers had an aperture of 13 mm and a focal length of 10 mm. They were made by lead zirconate titanate (PZT) ceramic piezo material (DL-47), which was purchased from Del Piezo Specialties LLC (West Palm Beach, FL, USA) at the cost of ~$80 per element. These miniaturized transducers could provide sufficient output pressure because PZT is the most commonly used material for high-power ultrasound transmission. We chose elements with three different frequencies (Fig. 1(c)), 1.5 MHz, 3 MHz, and 6 MHz, to investigate the relationship between frequency and BBBO outcome. The manufacturing of these transducers was straightforward as it only required gluing two wires to the positive and negative electrodes of the piezoelectric element.

The FUS transducer element was then encapsulated in a 3D-printed housing using epoxy (Devcon Epoxy Adhesive, Devcon Corp., Danvers, MA). The back of the transducer directly contacted the air to form air backing. The transducers were then connected to a power amplifier coupled with a function generator. No electrical impedance matching was needed because the real part of the transducer impedance at the resonance frequency, as measured by an E5061A ENA Network Analyzer with the 85070E Dielectric Probe Kit (Agilent Technologies, Santa Clara, CA, USA), was in the range of 31 to 59 ohms, which was sufficiently close to 50 ohms needed for a perfect impedance match.

The design of the transducer housing is shown in Fig. 1(b), which was manufactured using a 3D printer (Ultimaking Ltd., Netherlands). The housing provided a coupling cone, which was filled with ultrasound gel when in use for acoustic coupling. Two pairs of magnets were used to enable simple attachment and detachment of the transducer from the adaptor. The adaptor connected the FUS transducer to the bar commonly used to hold needles for stereotactic injections.

In order to achieve precise targeting of the FUS transducer at a specific brain location, a pointer was manufactured by 3D printing (Fig. 1d(i)). The tip of the pointer indicated the geometrical focus of the FUS transducer. The procedure for aligning the FUS transducer to target a specific brain location was similar to the established stereotactic procedure. First, a dot was drawn on the mouse scalp to indicate the location of the bregma, which was visible through the scalp. The pointer was then placed in the holder, and its position was adjusted by the stereotactic frame to align with the dot (Fig. 1d(i)). Then, the pointer was switched to the

FUS transducer and was moved to the target location using its coordinates in reference to the bregma as determined in reference to the mouse brain atlas [41] (Fig. 1d(ii)).

B. Simulation and calibration of the FUS transducers

The acoustic pressure fields generated by the FUS transducers in a mouse head were simulated using a Matlab toolbox, k-Wave, a k-space pseudospectral method-based solver [42]. A mouse head was placed in a μCT scanner (Rigaku, Tokyo, Japan). The acquired CT images consisted of 512×512×679 voxels with a spatial resolution of 0.08 mm. The voxel spacing was less than 1/8 of the corresponding FUS transducer's wavelength (e.g., 0.12 mm for 1.5 MHz, 0.06 mm for 3 MHz, and 0.03 mm for 6 MHz). The simulation domain size (20.0 mm × 20.0 mm × 16.3 mm) was kept the same for all the frequencies. The 3D simulations were based on a non-elastic model. A temporal duration of 100 μs was used for each frequency in the simulations. The time steps were set as 22 ns for 1.5 MHz, 11 ns for 3.0 MHz, and 6 ns for 6.0 MHz to ensure that the Courant–Friedrichs–Lewy (CFL) stability factors used in all the simulations were within 0.3. The density and sound speed of the skull and brain tissue were converted from the Hounsfield units of the CT images using the function 'hounsfield2density' in the k-Wave toolbox. This function uses a piecewise linear fit to the data reported by Schneider and Mast [43]. The sound speed of the coupling gel was set to be the same as that of the water (1484 m/s).

Experimental calibration of each FUS transducer was performed in degassed water without and with three degassed *ex vivo* mouse skulls. The skulls were positioned in front of the transducer. The acoustic pressure fields were measured using a hydrophone (HGL-200, ONDA Corporation, Sunnyvale, CA), which was moved in 3D using a computer-controlled 3D stage (PK245–01AA, Velmex Inc., NY, USA). The transmission efficiency of each FUS transducer was measured by the ratio between the maximum peak negative pressures measured with and without the skull.

C. In vivo evaluation of FUS-BBBO

1) Animal experimental procedure—All animal procedures were reviewed and approved by the Institutional Animal Care and Use Committee of Washington University in St. Louis in accordance with the National Institutes of Health Guidelines for animal research. Adult female mice (IACUC protocol number: 21–0187, C57BL/6, 8 weeks old, female, Charles River Laboratory, Wilmington, MA, USA) were used in this study. A total of 36 mice were randomly assigned to 9 groups to evaluate FUS-BBBO using FUS transducers with different frequencies (1.5, 3.0, 6.0 MHz) and different pressures (0.20, 0.40, 0.57 MPa) at each frequency. The acoustic pressures were measured in a water tank with *ex vivo* mouse skulls. Prior to FUS sonication, animals were placed in the stereotaxic frame under isoflurane anesthesia (1.5–2% v/v isoflurane in oxygen). The fur on the mouse head was shaved using a hair removal cream while the skull and the scalp remained intact. Ultrasound gel was applied onto the exposed skin above the skull and inside the housing of the small transducer. Mice were placed on a heating pad throughout the experiment. A catheter was placed in the mouse tail vein for intravenous injection.

The desired brain target was selected to be a point in the left thalamus using the following coordinates: −1.94 mm in the anterior-posterior (AP) direction, −1.50 mm in the medial-lateral (ML) direction, and −3.30 mm in the dorsal-ventral (DV) direction relative to the bregma according to the mouse brain atlas. The desired target location was indicated by the yellow dot in the transverse view (Fig. 2(a)) and coronal view (Fig. 2(d)) of the mouse brain atlas. The FUS transducer was moved by the stereotactic frame to target the desired brain location. Then, a mixture of 1 mL/kg gadolinium (Dotarem, Guerbet, Aulnay sous Bois, France), 60 μL of 2% Evans Blue, and 10 μL/kg of Definity (Lantheus Medical Imaging, Billerica, MA, USA) was administered intravenously. It was followed by FUS sonication (pulse length 6.6 ms; pulse repetition frequency 5 Hz; duration 120 s) with different combinations of exposure frequency (1.5, 3.0, and 6.0 MHz) and pressure (0.20, 0.40, and 0.57 MPa). Approximately 5 minutes after FUS sonication ended, mice were imaged by a 4.7 T small animal MRI scanner (Agilent/Varian DirectDrive™ console, Agilent Technologies, Santa Clara, CA, USA). A T1-weighted gradient-echo sequence was used for contrast-enhanced MRI (CE-MRI) using the following parameters: repetition time/echo time: 166 ms/6.4 ms; section thickness: 0.5 mm; in-plane resolution: 0.125 × 0.125 mm; matrix size: 256 × 256; number of signal averages: 2; flip angle: 60°. The BBB opening outcome was quantified based on hyperenhancement on the T1-weighted images, which indicated the leakage of gadolinium, as the intravenously injected gadolinium could not cross an intact BBB [44]. Approximately 15 minutes after FUS sonication, mice were transcardially perfused with 0.01 M phosphate-buffered saline (PBS) followed by 4% paraformaldehyde. The mouse brains were then harvested and fixed in 4% paraformaldehyde.

2) Characterization of the targeting accuracy using MRI—The targeting accuracy of the stereotactic-guided FUS device was quantified by the offset between the desired target location and the centroid of the BBBO detected by CE-MRI. Representative post-treatment CE-MRI images of the mouse brain are shown in Fig. 2(b, e). The hyperenhanced regions in the brain indicate the leakage of the MR contrast agent into the brain parenchyma, which represents the BBB opening area. The centroid of the BBB opening area was determined by finding the geometrical center of hyperenhanced regions using Matlab. The offset between the coordinates used for targeting and the centroid of the BBB opening was calculated along three axes: medial-lateral (ML), anterior-posterior (AP), and dorsal-ventral (DV) corresponding to X-, Y-, and Z-axis in Cartesian coordinates, respectively.

3) Quantification of gadolinium delivery outcome—The left (FUS-treated) and right (non-treated) sides of the brain on each CE-MRI image were manually outlined and processed by the following two steps. First, a region to cover the whole non-treated right side of the brain was manually drawn, and three times standard deviation above the mean was calculated to represent the background intensity. Then, a region to cover the whole FUS-treated left side of the brain was manually drawn, and pixels with intensities above the background intensity were identified. Gadolinium delivery volume was calculated by the total number of the identified pixels in the FUS-treated side.

4) Quantification of Evans blue delivery outcome—Evans blue has been commonly used as a model drug for evaluating the FUS-BBBO drug delivery outcome [22], [25]. The harvested mouse brains after fixation were cut into 1-mm thick coronal sections using the mouse brain matrix (World Precision Instruments, Sarasota, FL, USA). Fluorescence images of brain sections were taken using a LI-COR imaging system (Pearl Trilogy; 700 Channel laser source (Ex 785 nm/Em 820 nm); resolution 85 μm) and analyzed using Matlab (Mathworks, Natick, MA, USA). Same to the quantification method described earlier for gadolinium delivery, a region of interest was manually drawn to cover the non-treated right side of the brain for each brain section. Three times standard deviation above the mean pixel intensity within the non-treated region was calculated to represent the background autofluorescence intensity. Then, a region of interest was manually drawn to cover the FUS-treated left side of the brain. Pixels with intensities above the background autofluorescence intensity were identified for each brain section. Evans blue delivery volume was calculated by the total number of pixels with enhanced fluorescence signal in all the brain sections. The mean fluorescence intensity of pixels with enhanced fluorescence signal in all the brain sections was calculated to represent the signal intensity of the delivered Evans blue.

5) FUS-BBBO safety analysis—Histologic examination was performed for all mice using hematoxylin and eosin (H&E) staining. After fluorescence imaging, brain slices containing the highest Evans blue fluorescence signal were cryoprotected in 30% sucrose and embedded at −20 °C. Brain slices were then sectioned into 5 μm coronal sections and stained with H&E. Bright-field images of stained sections were obtained using an all-in-one microscope (BZ-X810, Keyence, Osaka, Japan) coupled with 2× and 20× objectives.

6) Statistics analysis—Linear curve fitting was performed using OriginLab software (Origin, Massachusetts, USA) for the following four groups: (a) Evans blue volume v.s. CI; (b) Evans blue volume v.s. MI; (c) Evans blue intensity v.s. CI; and (d) Evans blue intensity v.s. MI. The coefficient of determination (R2) was calculated. All data are presented in the format of mean ± standard deviation. Statistical significance was evaluated by the unpaired two-tailed student t-test using GraphPad Prism (Version 8.3, La Jolla, CA, USA), and $p\text{-value} < 0.05$ was defined as statistically significant.

III. RESULTS

A. Simulation and calibration of the FUS transducers with the mouse skull

Fig. 3(a) shows the transverse and coronal views of the simulated acoustic pressure fields transcranially at frequencies of 1.5, 3.0, and 6.0 MHz, respectively. Fig. 3(b) displays the experimental measurement results with the mouse skull. Fig. 3(c) presents the time-domain signals measured at the focus of three transducers with and without skull from simulation (Fig. 3c(i)) and experiments (Fig. 3c(ii)). Fig. 3(d) shows the beam profiles along the axial and lateral directions obtained from simulations (Fig. 3d(i)) and experiments (Fig. 3d(ii)). The focal region sizes defined by the full width at half maximum (FWHM) in axial and lateral directions are shown in Fig. 3(e). The simulation results showed that FUS focus was shifted by 0.3 mm along the axial direction toward the transducer at 6.0 MHz and 0.2 mm

at 3.0 MHz. The shift along the lateral direction was within 0.1 mm for all frequencies. Based on experimental measurement with only the top piece of the mouse skull, mouse skulls lead to less than 0.1 mm shift of the FUS focus in the axial and lateral directions at all frequencies. No standing wave was formed at 1.5 MHz because the hydrophone measurement was performed with only the top piece of the mouse skull. Based on the simulation results, as the FUS frequency increased from 1.5 MHz to 3.0 MHz and 6.0 MHz, the FWHM in the lateral direction decreased from 1.4 mm to 0.8 mm and 0.4 mm, respectively. According to the experimental measurements (Fig. 3e(i)), the FWHM in the axial direction decreased from 1.8 ± 0.1 mm to 1.0 ± 0.1 mm and 0.5 ± 0.0 mm, respectively. The FWHM in the axial direction decreased from 5.6 mm, 3.4 mm, to 2.2 mm in simulation and from 5.9 ± 0.1 mm, 3.6 ± 0.2 mm, to 3.0 ± 0.1 mm in calibration (Fig. 3e(ii)). The calculated focal volume based on ellipsoid volume equation ($V = 4\pi/3\ ab^2$, a and b are the half-width at half-maximum along axial and lateral direction respectively) decreased from 5.7 mm^3, 1.2 mm^3, to 0.2 mm^3 in simulation and from 9.7 ± 0.6 mm^3, 2.0 ± 0.1 mm^3, to 0.3 ± 0.0 mm^3 in calibration (Fig. 3e(iii)). The FUS transmission coefficient was 84.3 % for 1.5 MHz, 65.4 % for 3.0 MHz, 42.7% for 6.0 MHz based on simulation and 81.0% ± 4.2% for 1.5 MHz, 65.2% ± 2.1% for 3.0 MHz, 38.6% ± 2.2% for 6.0 MHz based on calibration (Figure 3e(iv)).

B. Targeting accuracy of the stereotactic-guided FUS device

Fig. 4 shows the accuracy of BBBO using the stereotactic-guided FUS device. The targeting accuracy for two groups treated using the 3.0 MHz transducer at 0.2 MPa, and the 6.0 MHz transducer at 0.2 MPa were excluded in the quantification because these two groups did not induce detectable BBBO. The targeting offset in X-, Y-, Z-axis were measured respectively to be −0.28 ± 0.23 mm, −0.04 ± 0.42 mm, 0.10 ± 0.32 mm for 1.5 MHz, 0.19 ± 0.37 mm, −0.21 ± 0.43 mm, −0.43 ± 0.17 mm for 3.0 MHz, and −0.31 ± 0.12 mm, −0.27 ± 0.28 mm, −0.27 ± 0.31 mm for 6 MHz. The absolute Euclidean distance was quantified to be 0.57 ± 0.18 mm for 1.5 MHz, 0.75 ± 0.09 mm for 3.0 MHz, and 0.60 ± 0.23 mm for 6 MHz (Fig. 4(b)) with no significant difference among different frequencies. The targeting offset of all groups combined was 0.63 ± 0.19 mm (Fig. 4(c)).

C. Gadolinium delivery outcome

MRI images in transverse and coronal views at different FUS frequencies and pressures are shown in Fig. 5(a). Gadolinium leakage was observed at 0.4 MPa and 0.57 MPa for all frequencies and 0.2 MPa for 1.5 MHz, whereas it was not detectable for 3.0 MHz and 6.0 MHz at 0.2 MPa. A summary of the mean gadolinium delivery volume for all the FUS-treated groups is shown in Fig. 5(b). The correlations between gadolinium delivery volume with CI and MI are shown in Fig. 5(c) and 5(d). A strong linear correlation was found between the gadolinium delivery volume and CI (R^2=0.92). The correlation of MI with gadolinium delivery volume was slightly lower (R^2=0.83).

D. Evans blue delivery outcome

Bright-field images of coronal sections of the mouse brains and corresponding fluorescence images are presented in Fig. 6(a). Evans blue extravasation was observed at 0.4 MPa and 0.57 MPa for all frequencies and 0.2 MPa for 1.5 MHz, whereas it was not detectable for

3.0 MHz and 6.0 MHz at 0.2 MPa. A summary of the mean Evans blue delivery volume and signal intensity for all the FUS-treated groups is shown in Fig. 6(b). The largest BBB opening volume was achieved at 1.5 MHz at a pressure of 0.57 MPa (Fig. 6(b)). The smallest BBB opening volume was achieved using 6 MHz with a pressure of 0.4 MPa.

The correlation between Evans blue delivery volume and signal intensity with CI is shown in Fig. 6(a) and 6(c). The correlation between Evans blue delivery volume and signal intensity with MI is shown in Fig. 6(b) and 6(d). A strong linear correlation was found between the Evans blue volume and CI (R^2=0.91). The correlation of MI with Evans blue volume was slightly lower (R^2=0.84). The correlation between Evans blue signal intensity and CI (R^2=0.68) was comparable to that with MI (R^2=0.71).

E. Safety analysis

Of all groups tested, we only detected microhemorrhage in 2 mice treated by 1.5 MHz at 0.57 MPa, corresponding to CI = 0.38 and MI = 0.46. Representative slides with microhemorrhage observed are shown in Fig. 7(a). No tissue damage was detected in other groups (Fig. 7(b) and 7(c)).

IV. DISCUSSION

This study presented an affordable and easy-to-use FUS device for spatially accurate, precise, and tunable drug delivery to the mouse brain.

This device has the following features. (1) The FUS transducer elements are widely available at a low cost (~$80 per element). Transducer manufacturing only required connecting wires to the electrodes on the elements. All other components can be 3D printed. We uploaded the open-source 3D printing file and permitted free access at https://github.com/ChenUltrasoundLabWUSTL/stereotactic-system.git. (2) The integration of the FUS transducers with a stereotactic frame for targeting desired brain location using established stereotactic procedures decreased the barrier to adopting the FUS technique. The device achieved sub-millimeter targeting accuracy. (3) The use of higher frequency FUS transducers (3.0 MHz and 6.0 MHz) decreased the BBBO volume and improved the spatial precision of FUS-BBBO in targeting individual structures in the mouse brain. (4) The drug delivery outcome was tunable by adjusting the CI or MI. We expect this device could be manufactured by research groups without ultrasound background and used in various applications with minimal training needed.

The targeting accuracy of the stereotactic-guided FUS system was high, reaching 0.63 ± 0.19 mm (Fig. 4(c)). Previous studies have reported the targeting accuracy of other FUS systems. For example, Chopra *et al.* developed an MRI-compatible, computer-controlled three-axis positioning system and reported a targeting accuracy of 0.29 ± 0.08 mm in gel phantom based on benchtop characterization [45]. The targeting accuracy of this system inside an MRI scanner was found to be 0.36 ± 0.14 mm by melting polystyrene plastic at the FUS focus, as reported by Ellens *et al.* [46]. Magnin *et al.* developed an MR-guided motorized FUS system and reported targeting accuracy within 0.5 mm in the rat brain *in vivo* [29]. The targeting offset of Bing *et al.*'s stereotaxic-guided FUS system was reported

to be around ±0.3 mm in the rat brain based on Evans blue extravasation after FUS-BBBO [24]. The targeting accuracy of our proposed system (0.63 ± 0.19 mm) is comparable to those reported in previous studies.

Multiple strategies have been proposed to improve the spatial precision of FUS in achieving BBBO in individual brain structures. One strategy is to replace a single-element FUS transducer with a phased array [47]–[49], including a small-aperture phased array that is currently under development for small animal experiments [30], but the high cost and complexity of a phased array limits its broad adoption. Other strategies include the use of two transducers with frequency-modulated crossed beams [50] and the use of chirp and random frequency-modulated ultrasound waveforms [51]. The focal region size of a single-element FUS transducer can be approximately estimated using $\lambda(F\#)$ in the lateral direction and $7\lambda\ (F\#)^2$ in the axial direction, where λ is the wavelength and $F\#$ =focal length/aperture [52]. It is well-known that increasing the transducer frequency can decrease the focal region size. We demonstrated that under the same pressure level, a higher frequency FUS transducer achieved a small drug delivery volume (Figs. 5 and 6), which improved the spatial precision of FUS-BBBO compared with that achieved with lower frequency transducers. There is a potential concern that the skull can distort the beam at higher frequencies. We found that focused beam pattern was formed even in the presence of the skull at all frequencies (Figs. 3(a) and 3(b)). The mouse skull only led to < 0.3 mm shift in the axial direction and < 0.1 mm in the lateral direction at all three frequencies based on simulations (Fig. 3(c)). Although the skull contributed to 17–61% attenuation of the acoustic pressure at 1.5–6.0 MHz, the skull attenuation was easily compensated by increasing the amplitude of the driving signal. The finding that the targeting accuracy of the FUS device was independent of the FUS frequency (Fig. 4) further indicate that the effect of the skull did not lead to a significant shift of the focal point. It is worth pointing out that, if needed, new FUS transducers can be designed with lower $F\#$ to further decrease the focal region size.

The FUS-BBBO drug delivery outcome can be tuned by the CI and MI within the range investigated in this study. Strong linear correlations were found between gadolinium delivery volume and CI or MI (Fig. 5). Similar strong linear correlations were also found between Evans blue delivery volume and CI or MI and relatively lower correlations were found between the Evans blue signal intensity and CI or MI (Fig. 6). Using two FUS transducers at 0.4 MHz and 1 MHz, one previous study also found strong linear correlations between MI/CI and CE-MRI signal intensity changes [40]. Our findings suggest that these strong correlations can be expanded to FUS-BBBO at higher frequencies, further confirming that CI and MI can be used to predict the FUS-BBBO drug delivery outcome. Although both CI and MI had linear correlations with the BBB opening volume, CI is a better indicator for BBB opening volume because the correlation coefficient of CI was higher than MI (0.92 for CI vs. 0.83 for MI based on gadolinium delivery; 0.91 for CI vs. 0.84 for MI based on Evans blue delivery).

This study has several limitations. Firstly, in order to minimize the barrier for the adoption of our device by the broad research community, our device did not include a passive cavitation detector, which can be used to monitor microbubble cavitation during FUS sonication [53]. If needed, a hole can be drilled in the center of the FUS transducer for inserting a

needle-shaped ultrasound sensor for cavitation monitoring. Secondly, the BBBO volume was increased by increasing CI and MI; however, the risk of tissue damage also increased as CI and MI increased. Tissue damage was observed at CI = 0.38 and MI = 0.46. Large BBBO volume can be achieved using multi-point sonication with each sonication within the safety range (CI < 0.38 or MI < 0.46). Future studies will investigate large-volume BBBO using a motorized stereotaxic frame for multi-point sonication via automatic mechanical movement of the transducer. Thirdly, the driving system used in our study was composed of a commercially available function generator and power amplifier. They are relatively bulky and expensive (~$10,000 in total). We used them in our study because they are readily available in our lab. Future studies can explore the use of low-cost signal generators and amplifiers to decrease the cost of the driving system.

V. CONCLUSION

In this study, we presented an affordable and easy-to-use FUS device for spatially accurate, precision, and tunable drug delivery to the mouse brain. This device integrated in-house manufactured miniature FUS transducers with a commercially available stereotactic frame for accurate brain targeting using established stereotactic procedures. This affordable, easy-to-use FUS device also achieved FUS-BBBO with high spatial precision, enabling precise targeting of specific brain structures. We showed that the drug delivery volume was found to be linearly correlated with CI and MI, and an even higher linear correlation with CI, suggesting that CI may be more accurate to predict the drug delivery volume induced by FUS-BBBO. Overall, this device can be used to regulate BBB permeability and deliver biochemical molecules to desired brain regions in mice. This device will significantly lower the barrier to adopting the FUS-BBBO technique by the broad research community.

Acknowledgments

This work was supported in part by the National Institutes of Health grants (R01EB027223, R01EB030102, and R01MH116981), the Office of Naval Research (grant number # N00014-19-1-2335), the Charlie Teo Foundation, and Little Legs Foundation.

REFERENCES

[1]. Haumann R, Videira JC, Kaspers GJL, van Vuurden DG, and Hulleman E, “Overview of Current Drug Delivery Methods Across the Blood–Brain Barrier for the Treatment of Primary Brain Tumors,” CNS Drugs, vol. 34, no. 11. Adis, pp. 1121–1131, Nov-2020, doi: 10.1007/s40263-020-00766-w. [PubMed: 32965590]

[2]. Park SH et al. , “Safety and feasibility of multiple blood-brain barrier disruptions for the treatment of glioblastoma in patients undergoing standard adjuvant chemotherapy,” J. Neurosurg, pp. 1–9, Jan. 2020, doi: 10.3171/2019.10.JNS192206.

[3]. Carpentier A et al. , “Clinical trial of blood-brain barrier disruption by pulsed ultrasound,” Sci. Transl. Med, vol. 8, no. 343, Jun. 2016, doi: 10.1126/scitranslmed.aaf6086.

[4]. Beccaria K et al. , “Ultrasound-induced blood-brain barrier disruption for the treatment of gliomas and other primary CNS tumors,” Cancer Lett, vol. 479, no. December 2019, pp. 13–22, 2020, doi: 10.1016/j.canlet.2020.02.013. [PubMed: 32112904]

[5]. Chen K-T et al. , “Neuronavigation-guided focused ultrasound (NaviFUS) for transcranial blood-brain barrier opening in recurrent glioblastoma patients: clinical trial protocol,” Ann. Transl. Med, vol. 8, no. 11, pp. 673–673, 2020, doi: 10.21037/atm-20-344. [PubMed: 32617293]

[6]. Gasca-Salas C et al. , “Blood-brain barrier opening with focused ultrasound in Parkinson’s disease dementia,” Nat. Commun, vol. 12, no. 1, pp. 1–7, 2021, doi: 10.1038/s41467-021-21022-9. [PubMed: 33397941]

[7]. Abrahao A et al. , “First-in-human trial of blood–brain barrier opening in amyotrophic lateral sclerosis using MR-guided focused ultrasound,” Nat. Commun, vol. 10, no. 1, pp. 1–9, 2019, doi: 10.1038/s41467-019-12426-9. [PubMed: 30602773]

[8]. Mehta RI et al. , “Blood-brain barrier opening with MRI-guided focused ultrasound elicits meningeal venous permeability in humans with early Alzheimer disease,” Radiology, vol. 298, no. 3, pp. 654–662, 2021, doi: 10.1148/radiol.2021200643. [PubMed: 33399511]

[9]. D’Haese PF et al. , “β-Amyloid Plaque Reduction in the Hippocampus After Focused Ultrasound-Induced Blood–Brain Barrier Opening in Alzheimer’s Disease,” Front. Hum. Neurosci, vol. 14, no. October, pp. 1–5, 2020, doi: 10.3389/fnhum.2020.593672. [PubMed: 32116598]

[10]. Lipsman N et al. , “Blood–brain barrier opening in Alzheimer’s disease using MR-guided focused ultrasound,” Nat. Commun, vol. 9, no. 1, pp. 1–8, 2018, doi: 10.1038/s41467-018-04529-6. [PubMed: 29317637]

[11]. Rezai AR et al. , “Noninvasive hippocampal blood−brain barrier opening in Alzheimer’s disease with focused ultrasound,” Proc. Natl. Acad. Sci. U. S. A, vol. 117, no. 17, pp. 9180–9182, 2020, doi: 10.1073/pnas.2002571117. [PubMed: 32284421]

[12]. Wang S et al. , “Noninvasive, focused ultrasound-facilitated gene delivery for optogenetics,” Sci. Rep, vol. 7, p. 39955, 2017, doi: 10.1038/srep39955. [PubMed: 28059117]

[13]. Szablowski JO, Lee-Gosselin A, Lue B, Malounda D, and Shapiro MG, “Acoustically targeted chemogenetics for the noninvasive control of neural circuits,” Nat. Biomed. Eng, vol. 2, no. 7, pp. 475–484, 2018, doi: 10.1038/s41551-018-0258-2. [PubMed: 30948828]

[14]. Todd N et al. , “Modulation of brain function by targeted delivery of GABA through the disrupted blood-brain barrier.,” Neuroimage, vol. 189, no. January, pp. 267–275, 2019, doi: 10.1016/j.neuroimage.2019.01.037. [PubMed: 30659957]

[15]. Liu H-L et al. , “Blood-brain barrier disruption with focused ultrasound enhances delivery of chemotherapeutic drugs for glioblastoma treatment.,” Radiology, vol. 255, no. 2, pp. 415–25, May 2010, doi: 10.1148/radiol.10090699. [PubMed: 20413754]

[16]. Kinoshita M, McDannold N, Jolesz FA, and Hynynen K, “Noninvasive localized delivery of Herceptin to the mouse brain by MRI-guided focused ultrasound-induced blood-brain barrier disruption,” Proc. Natl. Acad. Sci. U. S. A, vol. 103, no. 31, pp. 11719–11723, 2006, doi: 10.1073/pnas.0604318103. [PubMed: 16868082]

[17]. Liu HL et al. , “Focused ultrasound enhances central nervous system delivery of bevacizumab for malignant glioma treatment,” Radiology, vol. 28, no. 1, p. 152444, 2016, doi: 10.1148/radiol.2016152444.

[18]. Zhang X et al. , “Magnetic Resonance Imaging-Guided Focused Ultrasound-Based Delivery of Radiolabeled Copper Nanoclusters to Diffuse Intrinsic Pontine Glioma,” ACS Appl. Nano Mater, 2020, doi: 10.1021/acsanm.0c02297.

[19]. Curley CT et al. , “Augmentation of brain tumor interstitial flow via focused ultrasound promotes brain-penetrating nanoparticle dispersion and transfection,” Sci. Adv, vol. 6, no. 18, 2020, doi: 10.1126/sciadv.aay1344.

[20]. Leinenga G and Gotz J, “Scanning ultrasound removes amyloid- and restores memory in an Alzheimer’s disease mouse model,” Sci. Transl. Med, vol. 7, no. 278, pp. 278ra33–278ra33, 2015, doi: 10.1126/scitranslmed.aaa2512.

[21]. Hsu P-H et al. , “Focused Ultrasound-Induced Blood-Brain Barrier Opening Enhances GSK-3 Inhibitor Delivery for Amyloid-Beta Plaque Reduction,” Sci. Rep, vol. 8, no. 1, p. 12882, Dec. 2018, doi: 10.1038/s41598-018-31071-8. [PubMed: 30150769]

[22]. Yang Y, Pacia CP, Ye D, Yue Y, Chien CY, and Chen H, “Static magnetic fields dampen focused ultrasound- mediated blood-brain barrier opening,” Radiology, vol. 300, no. 3, p. 681, 2021, doi: 10.1148/radiol.2021204441. [PubMed: 34227880]

[23]. O’Reilly MA et al. , “Preliminary Investigation of Focused Ultrasound-Facilitated Drug Delivery for the Treatment of Leptomeningeal Metastases,” Sci. Rep, vol. 8, no. 1, p. 9013, Dec. 2018, doi: 10.1038/s41598-018-27335-y. [PubMed: 29899537]

[24]. Bing C, Ladouceur-Wodzak M, Wanner CR, Shelton JM, Richardson JA, and Chopra R, "Trans-cranial opening of the blood-brain barrier in targeted regions using astereotaxic brain atlas and focused ultrasound energy," J. Ther. Ultrasound, vol. 2, no. 1, pp. 1–11, 2014, doi: 10.1186/2050-5736-2-13. [PubMed: 25516803]

[25]. Ye D et al. , "Focused ultrasound-enabled delivery of radiolabeled nanoclusters to the pons," J. Control. Release, vol. 283, pp. 143–150, Aug. 2018, doi: 10.1016/j.jconrel.2018.05.039. [PubMed: 29864474]

[26]. Basavarajappa L, Rijal G, and Hoyt K, "Multifocused Ultrasound Therapy for Controlled Microvascular Permeabilization and Improved Drug Delivery," IEEE Trans. Ultrason. Ferroelectr. Freq. Control, vol. 68, no. 4, pp. 961–968, 2021, doi: 10.1109/TUFFC.2020.3026697. [PubMed: 32976098]

[27]. Poorman ME et al. , "Open-source, small-animal magnetic resonance-guided focused ultrasound system," J. Ther. Ultrasound, vol. 4, no. 1, pp. 1–16, 2016, doi: 10.1186/s40349-016-0066-7. [PubMed: 26788322]

[28]. Dervishi E et al. , "Transcranial high intensity focused ultrasound therapy guided by 7 TESLA MRI in a rat brain tumour model: A feasibility study," Int. J. Hyperth, vol. 29, no. 6, pp. 598–608, 2013, doi: 10.3109/02656736.2013.820357.

[29]. Magnin R et al. , "Magnetic resonance-guided motorized transcranial ultrasound system for blood-brain barrier permeabilization along arbitrary trajectories in rodents," J. Ther. Ultrasound, vol. 3, no. 1, pp. 1–11, 2015, doi: 10.1186/s40349-015-0044-5. [PubMed: 25635224]

[30]. Rahimi S, Jones RM, and Hynynen K, "A High-Frequency Phased Array System for Transcranial Ultrasound Delivery in Small Animals," IEEE Trans. Ultrason. Ferroelectr. Freq. Control, vol. 68, no. 1, pp. 127–135, 2021, doi: 10.1109/TUFFC.2020.3012868. [PubMed: 32746231]

[31]. Choi JJ, Pernot M, Small SA, and Konofagou EE, "Noninvasive, transcranial and localized opening of the blood-brain barrier using focused ultrasound in mice," Ultrasound Med. Biol, vol. 33, no. 1, pp. 95–104, 2007, doi: 10.1016/j.ultrasmedbio.2006.07.018. [PubMed: 17189051]

[32]. Gorick CM et al. , "Sonoselective transfection of cerebral vasculature without blood–brain barrier disruption," Proc. Natl. Acad. Sci, vol. 117, no. 11, p. 201914595, 2020, doi: 10.1073/pnas.1914595117.

[33]. McDannold N, Zhang Y, and Vykhodtseva N, "The Effects of Oxygen on Ultrasound-Induced Blood–Brain Barrier Disruption in Mice," Ultrasound Med. Biol, vol. 43, no. 2, pp. 469–475, Feb. 2017, doi: 10.1016/J.ULTRASMEDBIO.2016.09.019. [PubMed: 27789044]

[34]. Bing C et al. , "Characterization of different bubble formulations for blood-brain barrier opening using a focused ultrasound system with acoustic feedback control," Sci. Rep, vol. 8, no. 1, pp. 1–12, 2018, doi: 10.1038/s41598-018-26330-7. [PubMed: 29311619]

[35]. Liu HL et al. , "Design and experimental evaluation of a 256-channel dual-frequency ultrasound phased-array system for transcranial blood-brain barrier opening and brain drug delivery," IEEE Trans. Biomed. Eng, vol. 61, no. 4, pp. 1350–1360, 2014, doi: 10.1109/TBME.2014.2305723. [PubMed: 24658258]

[36]. Fan CH et al. , "Contrast-enhanced ultrasound imaging for the detection of focused ultrasound-induced blood-brain barrier opening," Theranostics, vol. 4, no. 10, pp. 1014–1025, 2014, doi: 10.7150/thno.9575. [PubMed: 25161701]

[37]. Xia J, Tsui PH, and Liu HL, "Low-pressure burst-mode focused ultrasound wave reconstruction and mapping for blood-brain barrier opening: A preclinical examination," Sci. Rep, vol. 6, no. June, pp. 1–11, 2016, doi: 10.1038/srep27939. [PubMed: 28442746]

[38]. Bing KF, Howles GP, Qi Y, Palmeri ML, and Nightingale KR, "Blood-Brain Barrier (BBB) Disruption Using a Diagnostic Ultrasound Scanner and Definity® in Mice," Ultrasound Med. Biol, vol. 35, no. 8, pp. 1298–1308, 2009, doi: 10.1016/j.ultrasmedbio.2009.03.012. [PubMed: 19545939]

[39]. McDannold N, Vykhodtseva N, and Hynynen K, "Blood-Brain Barrier Disruption Induced by Focused Ultrasound and Circulating Preformed Microbubbles Appears to Be Characterized by the Mechanical Index," Ultrasound Med. Biol, vol. 34, no. 5, pp. 834–840, 2008, doi: 10.1016/j.ultrasmedbio.2007.10.016. [PubMed: 18207311]

[40]. Chu PC, Chai WY, Tsai CH, Kang ST, Yeh CK, and Liu HL, "Focused Ultrasound-Induced Blood-Brain Barrier Opening: Association with Mechanical Index and Cavitation Index Analyzed by Dynamic Contrast-Enhanced Magnetic-Resonance Imaging," Sci. Rep, vol. 6, no. 1, p. 33264, Dec. 2016, doi: 10.1038/srep33264. [PubMed: 27630037]

[41]. Paxinos G and Franklin KBJ, Paxinos and Franklin's the Mouse Brain in Stereotaxic Coordinates, vol. 2nd Editio. Academic Press, 2001.

[42]. Treeby BE and Cox BT, "k-Wave: MATLAB toolbox for the simulation and reconstruction of photoacoustic wave fields," J. Biomed. Opt, vol. 15, no. 2, p. 021314, 2010, doi: 10.1117/1.3360308. [PubMed: 20459236]

[43]. Schneider U, Pedroni E, and Lomax A, "The calibration of CT Hounsfield units for radiotherapy treatment planning," Phys. Med. Biol, vol. 41, no. 1, pp. 111–124, 1996, doi: 10.1088/0031-9155/41/1/009. [PubMed: 8685250]

[44]. Yang Y, Pacia CP, Ye D, Yue Y, Chien C-Y, and Chen H, "Static Magnetic Fields Dampen Focused Ultrasound–mediated Blood-Brain Barrier Opening," Radiology, no. 21, p. 204441, 2021, doi: 10.1148/radiol.2021204441.

[45]. Chopra R, Curiel L, Staruch R, Morrison L, and Hynynen K, "An MRI-compatible system for focused ultrasound experiments in small animal models," Med. Phys, vol. 36, no. 5, pp. 1867–1874, 2009, doi: 10.1118/1.3115680. [PubMed: 19544806]

[46]. Ellens NPK et al. , "The targeting accuracy of a preclinical MRI-guided focused ultrasound system," Med. Phys, vol. 42, no. 1, pp. 430–439, 2015, doi: 10.1118/1.4903950. [PubMed: 25563283]

[47]. K H et al. , "500-element ultrasound phased array system for noninvasive focal surgery of the brain: a preliminary rabbit study with ex vivo human skulls," Magn. Reson. Med, vol. 52, no. 1, pp. 100–107, 2004, doi: 10.1002/MRM.20118. [PubMed: 15236372]

[48]. J S, A P, Y H, and K H, "Investigation of standing-wave formation in a human skull for a clinical prototype of a large-aperture, transcranial MR-guided focused ultrasound (MRgFUS) phased array: an experimental and simulation study," IEEE Trans. Biomed. Eng, vol. 59, no. 2, pp. 435–444, Feb. 2012, doi: 10.1109/TBME.2011.2174057. [PubMed: 22049360]

[49]. GT C, J S, T G, and K H, "A hemisphere array for noninvasive ultrasound brain therapy and surgery," Phys. Med. Biol, vol. 45, no. 12, pp. 3707–3719, 2000, doi: 10.1088/0031-9155/45/12/314. [PubMed: 11131194]

[50]. Sun T et al. , "Closed-loop control of targeted ultrasound drug delivery across the blood–brain/tumor barriers in a rat glioma model," Proc. Natl. Acad. Sci, vol. 114, no. 48, pp. E10281–E10290, 2017, doi: 10.1073/pnas.1713328114. [PubMed: 29133392]

[51]. Kamimura HAS et al. , "Chirp- and random-based coded ultrasonic excitation for localized blood-brain barrier opening.," Phys. Med. Biol, vol. 60, no. 19, pp. 7695–712, 2015, doi: 10.1088/0031-9155/60/19/7695. [PubMed: 26394091]

[52]. Hunt JW, Arditi M, and Foster FS, "Ultrasound Transducers for Pulse-Echo Medical Imaging," IEEE Trans. Biomed. Eng, vol. BME-30, no. 8, pp. 453–481, 1983, doi: 10.1109/TBME.1983.325150.

[53]. O'Reilly MA and Hynynen K, "Blood-brain barrier: Real-time feedback-controlled focused ultrasound disruption by using an acoustic emissions-based controller," Radiology, vol. 263, no. 1, pp. 96–106, 2012, doi: 10.1148/radiol.11111417. [PubMed: 22332065]

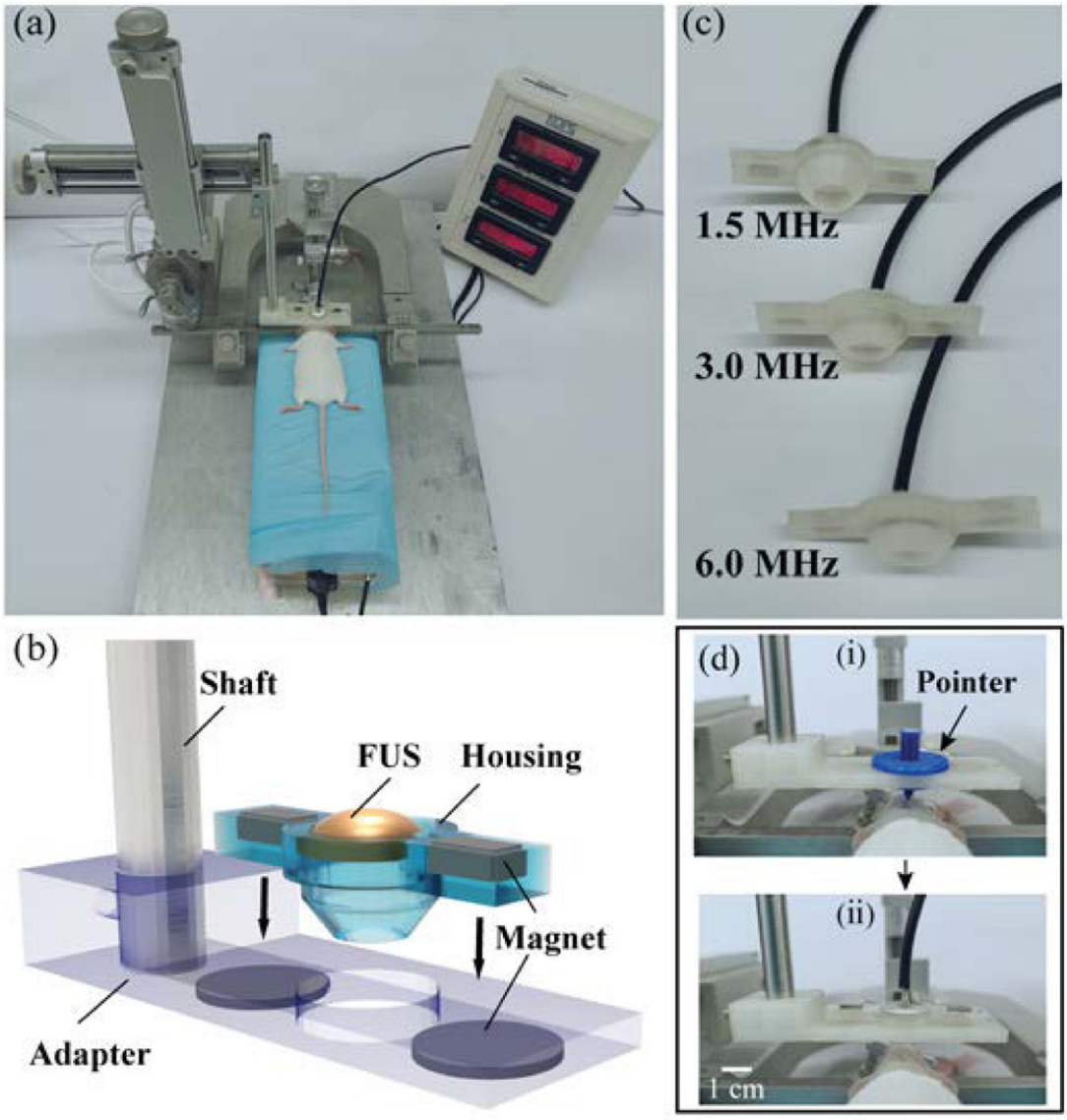

Fig. 1.

Stereotactic-guided FUS device. (a) Picture of the stereotactic-guided FUS system. (b) Ultrasound parts: FUS transducer, housing, and adapter. (c) FUS transducers with frequencies of 1.5, 3.0, and 6.0 MHz. (d) Brain targeting: (i) A 3D-printed pointer was aligned with the bregma in the mouse skull that was visible through the scalp, (ii) The pointer was then replaced by the FUS transducer and moved by the stereotactic frame to the targeted brain location using its coordinates in reference to the bregma as determined in reference to the mouse brain atlas.

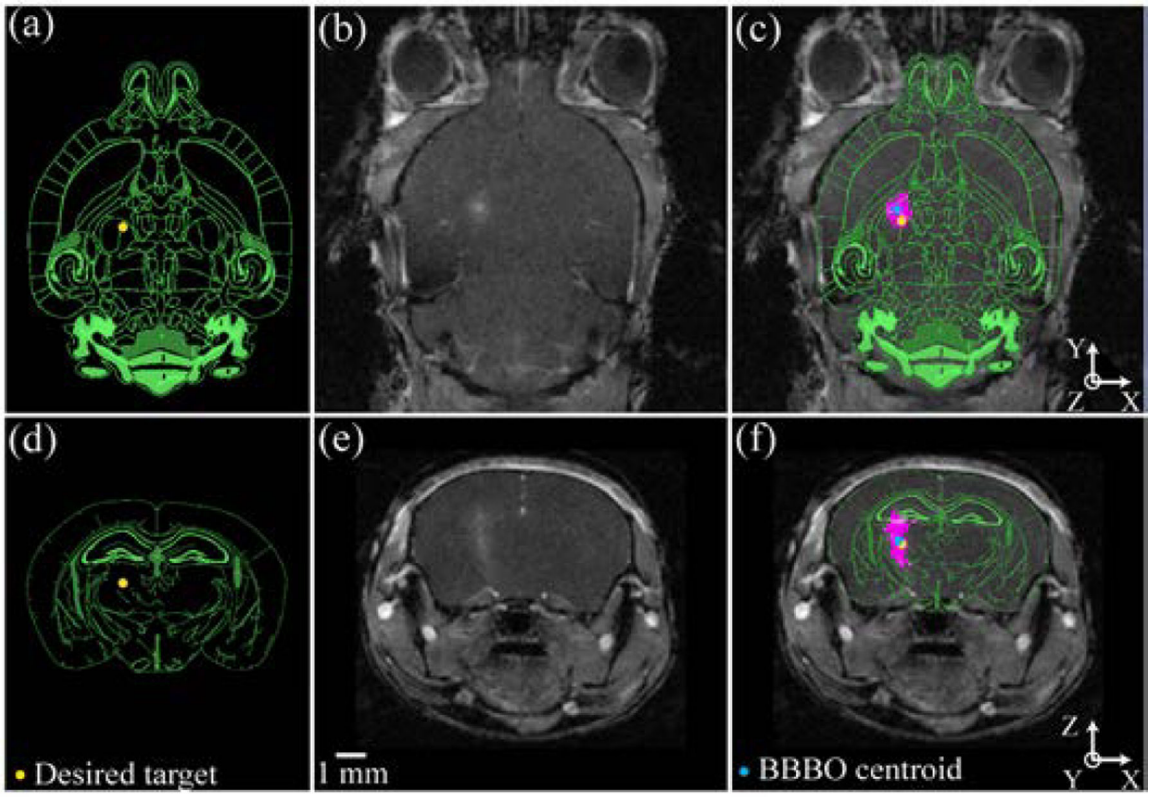

Fig. 2.

FUS targeting accuracy quantification. (a, d) The desired target location was indicated by a yellow dot in transverse and coronal views of the mouse brain atlas, respectively. (b, e) The contrast-enhanced MRI images of the mouse brain post-FUS treatment. (c, f) Co-registration of the mouse brain atlas with MRI images based on anatomic brain structures. The brain atlas is in green and the BBBO area is in purple. The centroid of the BBBO area is indicated by the blue dot.

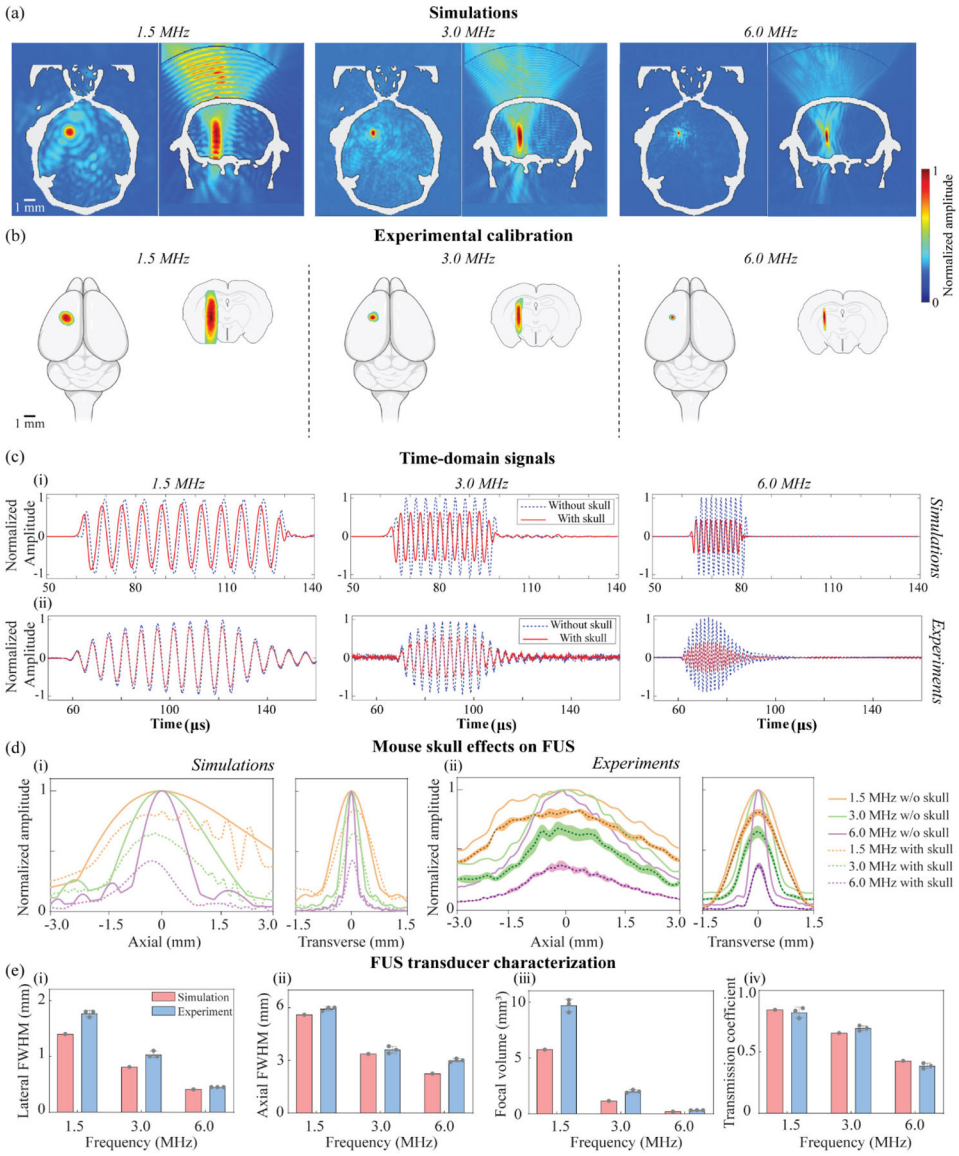

Fig. 3.

FUS transducer characterization by numerical simulation and experimental calibration. (a) Simulated ultrasound pressure fields in the transverse and coronal views for 1.5 MHz, 3.0 MHz, and 6.0 MHz FUS transducers, respectively. (b) Corresponding experimental measurements of the ultrasound pressure fields overlaid on illustrations of the mouse brain. (c) Time-domain signals measured at the focal point of different FUS transducers with and without skull based on simulations and experiments. (d) (i) Simulation and (ii) experimental measurement of the transcranial beam profiles along axial and lateral directions at each frequency. The shadow in (ii) indicates the standard deviation calculated based on measurements performed with three different skulls and each skull with three repeated measurements. (e) (i) Lateral FWHM diameter, (ii) Axial FWHM diameter, (iii) Focal volume, and (iv) Transcranial transmission ratio of the FUS transducers at different frequencies and with the mouse skull based on simulations and experiments.

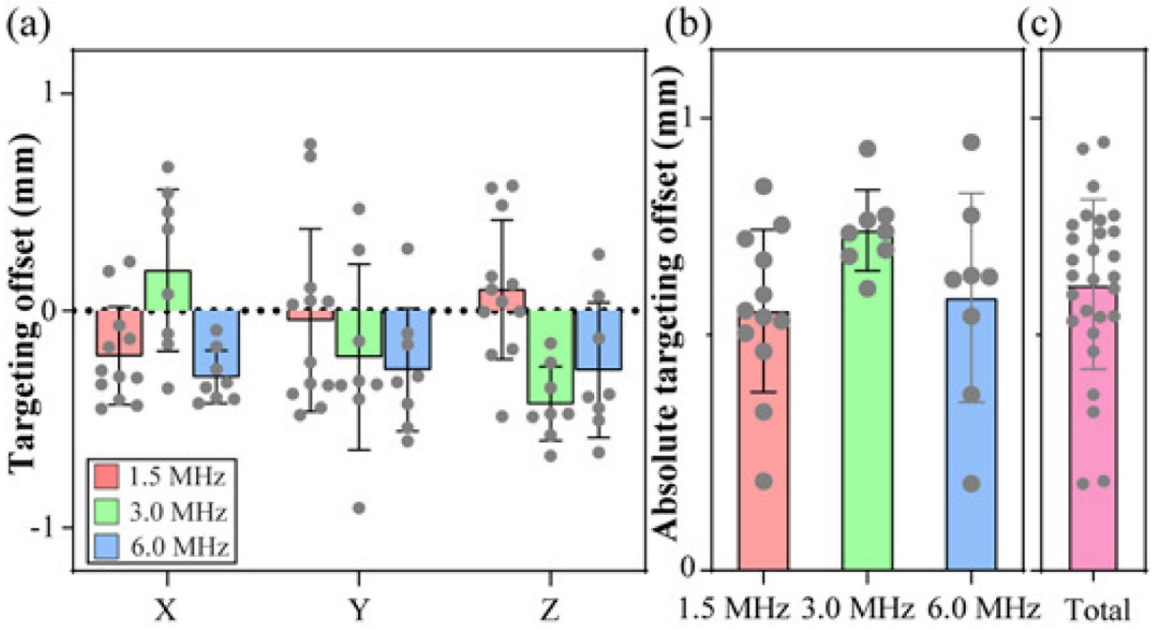

Fig. 4.

FUS device targeting accuracy. (a) The targeting offset along X-, Y-, Z-axis for mice treated at 1.5 MHz, 3.0 MHz, and 6.0 MHz (b) The absolute Euclidean distance of the targeting offset for different frequencies, and the absolute targeting offset was not significantly different among different frequencies. (c) The targeting offset of all groups. Error bars indicate the standard deviation.

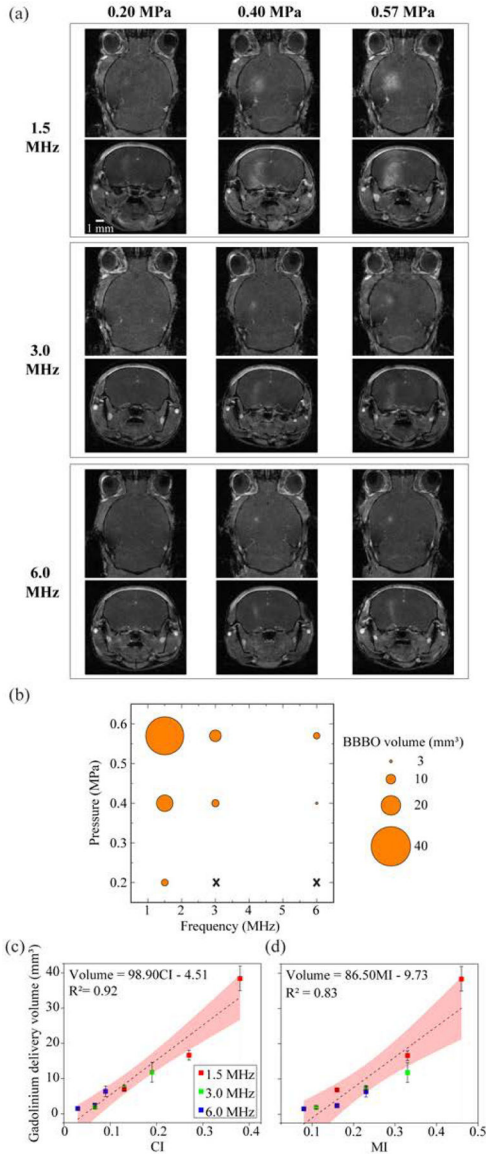

Fig. 5.

Gadolinium delivery outcome evaluation. (a) Transverse (upper) and coronal (bottom) views of CE-MRI images for representative mouse brains treated at different frequencies (1.5, 3.0, or 6.0 MHz) and pressures (0.2, 0.4, or 0.57 MPa). (b) A summary of the average gadolinium delivery volume for all groups. The variation of BBBO volume is indicated by the error bars in (c) and (d). Gadolinium leakage was not detectable in the groups marked by “x”. Strong linear correlations were found between gadolinium delivery volume and CI (c), as well as between gadolinium delivery volume and MI (d). Error bars indicate standard deviation. Shaded areas indicate the 95% confidence band of the linear fitting curves.

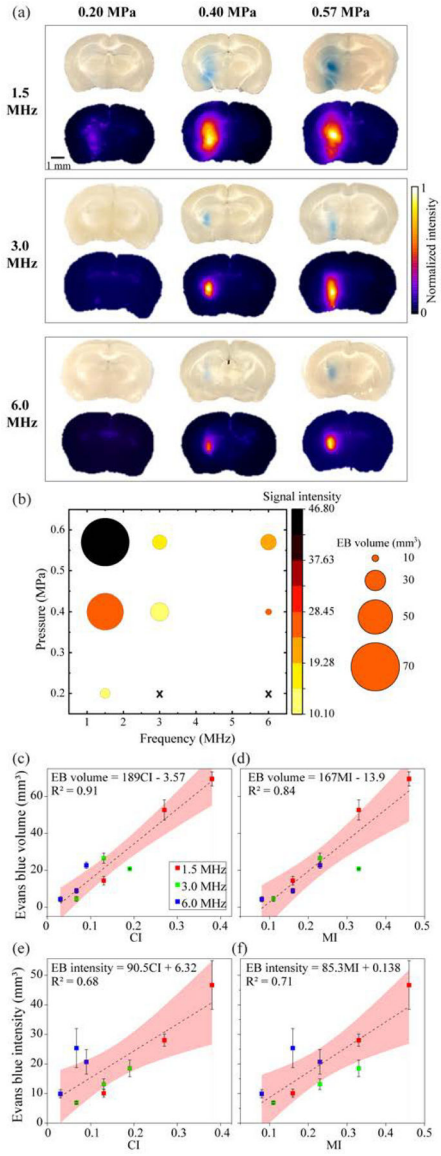

Fig. 6.

Evans blue delivery outcome evaluation. (a) Bright-field (upper) and corresponding fluorescence (bottom) images of coronal sections from representative mouse brains treated at different frequencies (1.5, 3.0, or 6.0 MHz) and pressures (0.20, 0.40, or 0.57 MPa). (b) A summary of the average Evans blue volume and signal intensity for all groups. The variation of BBBO volume and signal intensity are indicated by error bars in the (c-f). Evans blue was not detectable in the groups marked by “x”. The correlation between Evans blue volume and CI (c), Evans blue volume and MI (d), Evans blue signal intensity with CI (e), Evans blue signal intensity and MI (f). The equation shows the linear regression of the fitted curve, EB represents Evans blue. Error bars indicate standard deviation. Shaded areas indicate the 95% confidence interval of the fitting curves.

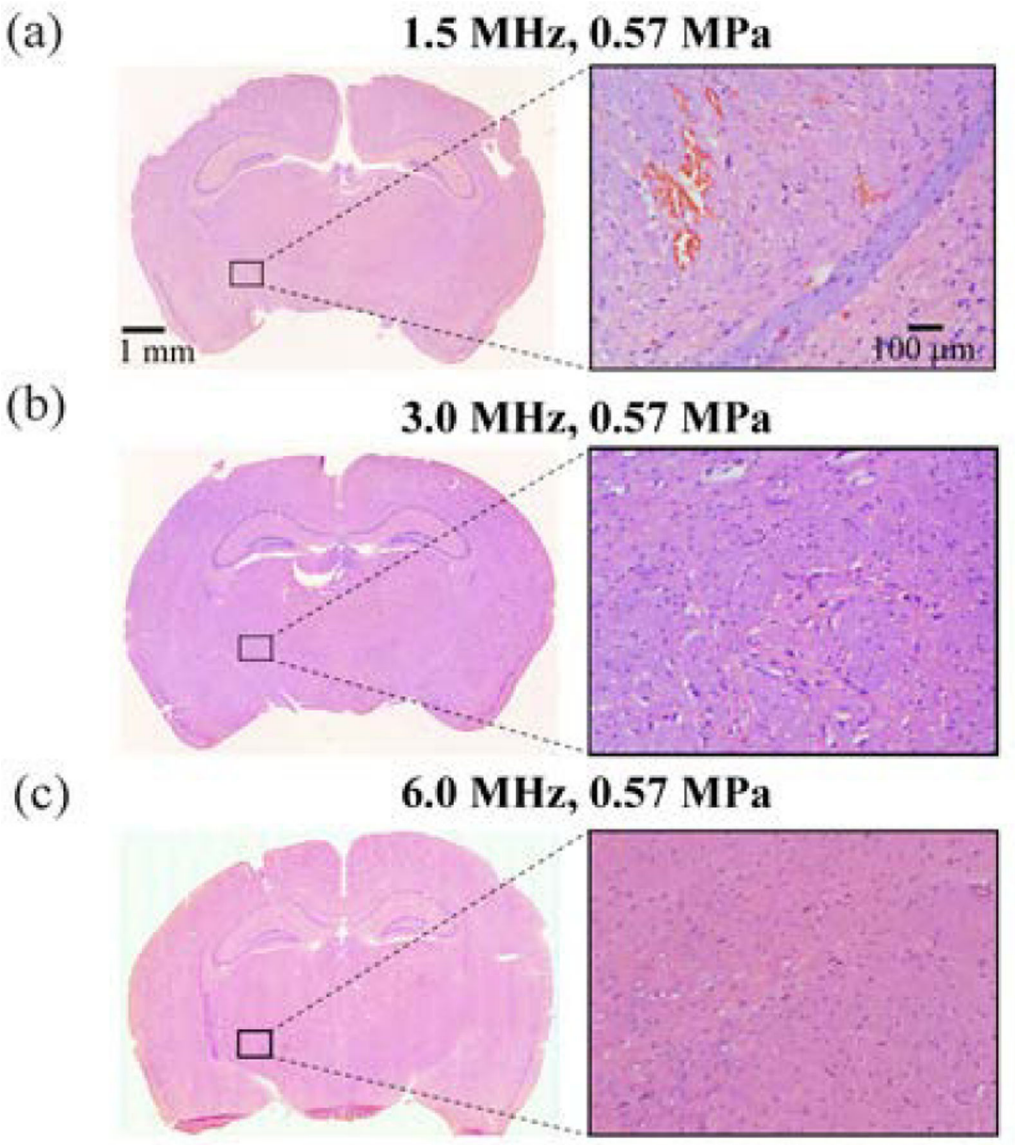

Fig. 7.

H&E-stained brain sections after FUS exposure at 0.57 MPa with 1.5 MHz (a), 3.0 MHz (b), and 6.0 MHz (c) at 0.57 MPa. Hemorrhage was observed at 1.5 MHz at 0.57 MPa but not at other conditions, as shown by the high magnification images.